

Optimization of material distribution in functionally graded structures with stress constraints

Fernando V. Stump¹, Emílio C. N. Silva^{1,*},[†] and Glaucio H. Paulino²

¹*Department of Mechatronics and Mechanical Systems Engineering, University of São Paulo, Prof. Mello Moraes Avenue, 2231 São Paulo, SP, Brazil*

²*Department of Civil and Environmental Engineering, Newmark Laboratory, University of Illinois at Urbana-Champaign, 205 North Mathews Avenue, MC-250, Urbana, IL 61801, U.S.A.*

SUMMARY

This work describes a topology optimization framework to design the material distribution of functionally graded structures considering mechanical stress constraints. The problem of interest consists in minimizing the volumetric density of a material phase subjected to a global stress constraint. Due to the existence of microstructure, the micro-level stress is considered, which is computed by means of a mechanical concentration factor using a p-norm of the Von Mises stress criterium (applied to the micro-level stress). Because a 0–1 (void–solid) material distribution is not being sought, the singularity phenomenon of stress constraint does not occur as long as the material at any point of the medium does not vanish and it varies smoothly between material 1 and material 2. To design a smoothly graded material distribution, a material model based on a non-linear interpolation of the Hashin–Strikhman upper and lower bounds is considered. Consistently with the framework adopted here in, the so-called ‘continuous approximation of material distribution’ approach is employed, which considers a continuous distribution of the design variable inside the finite element. As examples, the designs of functionally graded disks subjected to centrifugal body force are presented. The method generates smooth material distributions, which are able to satisfy the stress constraint. Copyright © 2006 John Wiley & Sons, Ltd.

Received 30 March 2006; Revised 30 June 2006; Accepted 5 July 2006

KEY WORDS: functionally graded materials; stress constraint; topology optimization

1. INTRODUCTION

Functionally graded materials (FGMs) present continuously graded properties and are characterized by spatially varying microstructures created by both non-uniform distribution of the reinforcement

*Correspondence to: Emílio C. N. Silva, Department of Mechatronics and Mechanical Systems Engineering, University of São Paulo, Prof. Mello Moraes Avenue, 2231 São Paulo, SP, Brazil.

[†]E-mail: ecnsilva@usp.br

Contract/grant sponsor: CNPq; contract/grant number: 131436/2004-0

Contract/grant sponsor: NSF; contract/grant number: CMS#0303492

phase and by interchanging the role of reinforcement and matrix (base) materials in a continuous way. The smooth variation of properties may offer advantages such as reduction of stress concentration and increased bonding strength. A major advantage of FGMs is the possibility of tailoring its gradation to maximize performance.

Due to the above features, some researchers have applied optimization methods to design FGMs. The work of Cho and Choi [1] presents a volumetric density optimization of each phase inside a domain considering the reduction of thermal stress levels. Taking into account the mechanical stress in functionally graded rotating disks, Durodola and Attia [2] and Horgan and Chan [3] present studies regarding stress distribution of rotating disks for different gradation of material properties. The work of Turteltaub [4] describes a study on the volumetric density optimization of FGMs to control the temperature field for transient loads. The application of a generic optimization method to tailor material property gradation was proposed by Paulino and Silva [5], who applied the topology optimization method framework to solve the problem of maximum stiffness design. Stump [6] applied this framework to solve a stress constrained problem.

Topology optimization is a powerful structural optimization method that seeks an optimal structural topology design by determining which parts of space should be solid and which parts should be void (i.e. no material) inside a given domain. The topology optimization method [7] has been successfully applied to a large range of problems (see Reference [8]). However, the 0–1 design is an ill-posed problem and a typical way to seek a solution for topology optimization problems is to relax the problem by defining a material model that allows for intermediate (composites) property values. In this sense, the relaxation yields a continuous material design problem that no longer involves a discernible connectivity. An actual topology solution can be obtained by applying penalization coefficients to the material model, and some complexity constraint of material distribution. Thus, the 0–1 design is recovered and also a discernible connectivity [8], characterizing a layout design. The relaxed problem is strongly related to the FGM design problem proposed in this work, which essentially seeks a continuous transition of material properties, to determine the material phase volumetric density of each point of the structure, so that a stress constraint is satisfied.

Duysinx and Bendsøe [9] have applied the topology optimization method to synthesize structures considering mechanical stress constraints. Due to difficulties that arise in the topology optimization formulation, stress constraints are still a challenge. The major problems are: the large number of constraints that must be considered in the optimization problem and the phenomena of stress singularities, which occurs in truss optimization [10], as well as in the continuum setting [9]. Some alternatives in dealing with the large number of constraints are the use the augmented Lagrangian optimization method [11] or the use a global stress index, e.g. p-norm, that characterizes the stress state in the structure [12]. A feasible treatment to the problem associated to the stress singularity phenomena is the ε relaxation method proposed by Cheng and Guo [13].

In this work, the design of optimized FGM structures considering stress constraints is proposed by using topology optimization based on a relaxed problem obtained by defining a material model for a two-phase FGM. Section 2 presents some basic concepts of topology optimization; Section 3 addresses the material model adopted to estimate the effective properties; Section 4 discusses computation of stresses accounting for material microstructure; Section 5 stipulates the overall problem formulation; Section 6 presents a few aspects of the numerical implementation; Section 7 provides numerical examples; and finally, Section 8 concludes the present work.

2. CONTINUUM TOPOLOGY OPTIMIZATION

The topology optimization method consists in solving a layout optimization problem by using a material distribution. The layout optimization of continuum structures determines the optimum external shape as well as the number, shape and positions of holes inside the structure regarding a given objective function. This problem is solved by defining an *extended design domain*, which is a large fixed domain that must contain the whole structure to be determined by the optimization procedure. It is usually discretized by finite elements, which allow the evaluation of the structure mechanical response. Because the finite element mesh is fixed, the calculation of derivatives of a continuous differentiable function inside the domain is simplified.

As indicated above, in order to obtain an engineering solution the problem is relaxed by allowing the material to assume intermediate property values during the optimization process, which can be achieved by defining a special material model [7]. The space of admissible solution is changed from a discrete one, which is described by a piecewise function with only zero or one values, to a continuum one where each point of the domain is represented by a composite with volumetric density changing continuously from zero to one. From a practical point of view, *material models* are functions that parametrize material constitutive tensor in terms of one or more continuum variables. To obtain a binary material distribution, these intermediate materials are subjected to penalization. These continuous numerical approximations of the binary material field are widely used in practical topology optimization implementations.

However, based on the concept of material model and the knowledge of dealing with the material distribution optimization problem applied to solve a layout optimization problem (see References [8, 14]), it is possible to propose a generic and robust method to deal with the optimization of functionally graded structures. Thus, this work focuses on applying the theoretical and numerical background developed for the topology optimization method to solve a two-phase material distribution optimization problem, with emphasis on the design of functionally graded structures.

An approach to define the material model consists of choosing a composite material, which means to define a microstructure, and then parametrize its unit cell. Thus, it is possible to obtain the constitutive tensor of the composite material at each point of the domain by applying the homogenization method. This is usually called ‘homogenization approach’ [15]. Another approach to obtain a material model is to define an empiric rule that parametrizes the constitutive tensor, such that the microstructure is not specified. In the topology optimization method, the most common technique is the SIMP (Solid Isotropic Microstructure with Penalization) [8]. In this work, a material model based on the Hashin–Shtrikman (HS) bounds is proposed.

In addition, the recent contributions of Matsui and Terada [16] and Rahmatalla and Swan [17] related to the implementation and discussion of the continuous approximation of material distribution (CAMD) are applied. Although those works are concerned with reducing the so-called checkerboard numerical instability in the discrete (0–1) problem, the continuous approximation of material distribution (CAMD) is closely related to the FGM concept, being the approach of choice to obtain a smooth material distribution. In the FGM literature, this concept was implemented to model graded structures originating the so-called ‘graded finite element’ [18].

3. A FUNCTIONALLY GRADED MATERIAL MODEL

The relaxed problem discussed above can be understood as a problem of optimal distribution of mechanical properties inside an *extended design domain*, instead of optimal distribution of material

itself. In this case, we may consider the *SIMP* model given in the form:

$$\mathbf{C}^{\text{Eff}} = \rho^p \mathbf{C}^+ + (1 - \rho^p) \mathbf{C}^- \quad (1)$$

This approach implies solving a distribution of mechanical properties bounded by the stiffness tensors \mathbf{C}^+ and \mathbf{C}^- . In this work, the superscripts $+$ and $-$ indicate the stiffer and softer material phases, respectively. The superscript notation is extended to all other variables to designate the associated phase. This approach is valid if there is interest in finding a component made of only two materials, i.e. material ‘plus’ or material ‘minus’, however, not composites or graded materials.

In the case of FGMs, this approach lacks physical meaning. If ρ is considered to be the volumetric density of material ‘plus’ (identified by the superscript ‘+’), the tensor \mathbf{C}^{Eff} cannot necessarily be realized with a mixture of materials with \mathbf{C}^+ and \mathbf{C}^- stiffness tensors [19]. Thus, to apply the topology optimization framework to the design of functionally graded structures, it is necessary to adopt a micromechanical model that represents an FGM made of two pre-defined materials.

In the literature, there are several material models applied to estimate the effective properties of composite materials. Those conventional models, such as Mori–Tanaka and self-consistent, have been applied to estimate the effective properties of FGM in the works of Zuiker and Dvorak [20], Reiter *et al.* [21], Reiter and Dvorak [22], Tanaka *et al.* [23] and Kim and Paulino [24]. However, they were originally developed for statistically homogeneous materials and are not able to capture the material gradient nature of the FGMs [25]. An alternative higher-order micromechanical theory has been proposed by Aboudi *et al.* [26].

A typical FGM microstructure is illustrated by Figure 1, where it is possible to see that, toward the gradation (top-down), there is a matrix zone (M^+) filled with discrete particle in a continuous matrix followed by a skeletal transition zone, where both phases are connected in a network and it is not possible to distinguish the matrix and particle phases. The transition zone is followed by

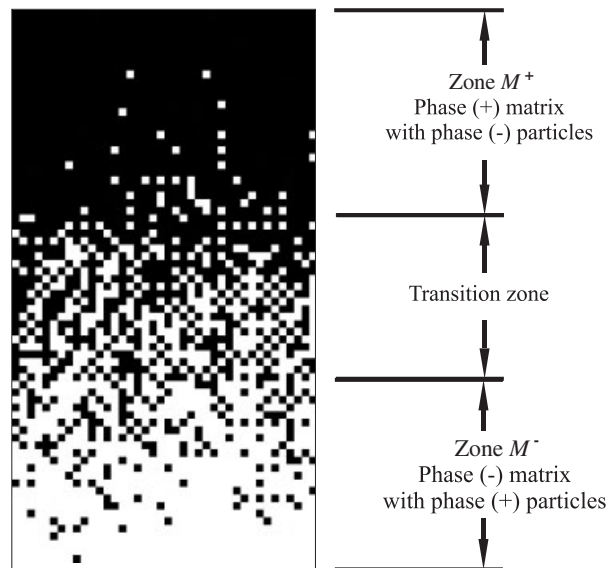


Figure 1. Schematic representation of an FGM.

another matrix zone (M^-) such as the first zone, however, with the role of matrix and particle interchanged.

Due to the continuous microstructural changes, the traditional concept of representative volume element (RVE) applied to conventional models remains to be justified [26]. Thus, focusing on this issue, some specific material models were developed to estimate the effective properties of FGMs. For instance, Yin *et al.* [27] developed a material model based on the Eshelby's equivalent inclusion method with pairwise particle interaction, and Aboudi *et al.* [26] developed a higher-order numerical cell theory. In this work, a rather simple and generic type of material model will be applied to estimate the effective properties of FGMs.

As motivation to our approach, we recall the work by Reiter and Dvorak [22], in which they propose a combination of the Mori–Tanaka method for the matrix-particle zones, and the self-consistent method for the skeletal zone. Here we consider simply a non-linear interpolation between the upper and lower HS bounds. In a more general approach, the HS bounds are considered as they are independent of the inclusion geometry. In addition, Benveniste [28] investigated a two-phase composite with spherical inclusions and isotropic constituents, and demonstrated that if the matrix is the softest phase the effective properties given by the Mori–Tanaka method are equal to the lower HS bound, and equal to the upper HS bound if the contrary occurs.

Thus, taking into account the gradient nature of FGMs, the lower HS bound is applied to the volumetric densities of phase + ranging from 0 to around 0.4, estimating the properties of zone M^- in Figure 1, and the upper HS bound is applied to densities ranging from around 0.6 to 1.0, estimating the M^+ zone. In the skeletal zone, with densities between 0.4 to 0.6, a continuous interpolation of the upper and lower HS bounds is applied.

The upper and lower H–S bounds for the bulk modulus (K_{upper} and K_{lower}) and the shear modulus (G_{upper} and G_{lower}) are given in the Appendix A. Thus, to consider a continuous transition between the lower and the upper bound, an interpolation of both bounds is applied and given by

$$K^H(\rho) = \varphi(\rho)K_{\text{upper}}(\rho) + (1 - \varphi(\rho))K_{\text{lower}}(\rho) \quad (2)$$

$$G^H(\rho) = \varphi(\rho)G_{\text{upper}}(\rho) + (1 - \varphi(\rho))G_{\text{lower}}(\rho) \quad (3)$$

where $\varphi(\rho)$ is given by recursive use of a function $\phi(\rho)$ given by

$$\phi(\rho) = \frac{\cos(\pi\rho)}{2} + \frac{1}{2} \quad (4)$$

so that $\varphi(\rho)$ is given by

$$\varphi(\rho) = \phi(\phi(\phi(\phi(\phi(\rho)))))) \quad (5)$$

With the material model defined above, it is possible to write the material constitutive ($\mathbf{C}^{\text{Eff}}(\rho)$) tensor as a function of the material volumetric density. To illustrate the material model employed the effective Young's modulus for material with $E^+ = 1$ and $E^- = 0.1$ is plotted and presented in Figure 2.

To consider body forces it is necessary to calculate the material density (ϱ) in terms of the material volumetric density (ρ) and the density of each phase (ϱ^+ and ϱ^-). Thus, the following relation is applied:

$$\varrho^{\text{Eff}} = \rho\varrho^+ + (1 - \rho)\varrho^- \quad (6)$$

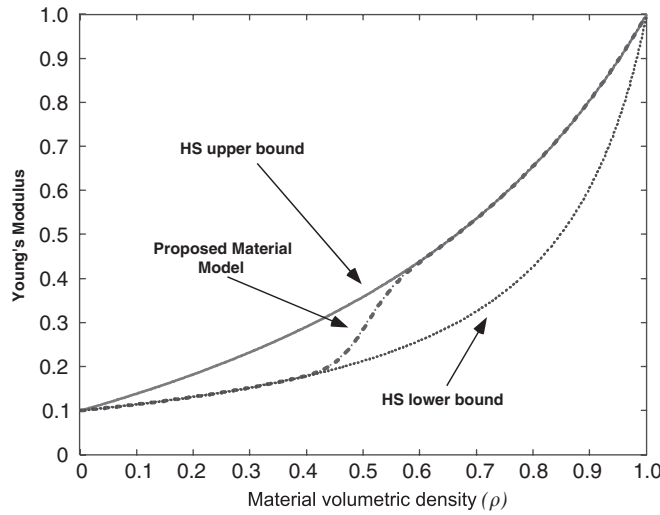


Figure 2. Young’s modulus for the proposed material model.

where ϱ^{Eff} indicates the homogenized material density, and ϱ^+ , ϱ^- denote the material densities of phases + and -, respectively.

In addition to the physical existence of the material obtained at the optimal solution, another important point to consider is how the stress is evaluated in the grey-scale regions. Thus, the stress constraint needs to be considered in the design problem, which is addressed next.

4. STRESS CRITERIA

The stress and strain fields evaluated considering the constitutive tensor $\mathbf{C}^{\text{Eff}}(\rho)$ represent a macro-stress field obtained under the assumption that the material is pointwise homogeneous. However, at the micro-scale level, the FGM is not homogeneous and the macro-stress (that is considered uniform over a RVE) must be evaluated separately for each material phase.

Considering the average stress and average strain theorems [26], the macro-stress and macro-strain fields are related to micro-stress and micro-strain fields by the following integral relations:

$$\langle \boldsymbol{\sigma} \rangle = \frac{1}{V} \int_V \boldsymbol{\sigma}(\mathbf{y}) dV = \boldsymbol{\sigma}^0, \quad \langle \boldsymbol{\varepsilon} \rangle = \frac{1}{V} \int_V \boldsymbol{\varepsilon}(\mathbf{y}) dV = \boldsymbol{\varepsilon}^0 \tag{7}$$

where V is the RVE volume, and $\langle \cdot \rangle$ represents the mean of the corresponding quantity. Thus, it is possible to define homogenized tensors which in the macro-scale follow the relation

$$\langle \boldsymbol{\sigma} \rangle = \mathbf{C}^{\text{Eff}} \langle \boldsymbol{\varepsilon} \rangle \tag{8}$$

From the hypothesis given in (7), for a two-phase material problem the average stresses and strains are given by

$$\langle \boldsymbol{\sigma} \rangle = \rho \langle \boldsymbol{\sigma}^+ \rangle + (1 - \rho) \langle \boldsymbol{\sigma}^- \rangle, \quad \langle \boldsymbol{\varepsilon} \rangle = \rho \langle \boldsymbol{\varepsilon}^+ \rangle + (1 - \rho) \langle \boldsymbol{\varepsilon}^- \rangle \tag{9}$$

respectively, where $\langle \cdot \rangle$ represents the mean of the corresponding value over the material phase. The pointwise constitutive relations in the microstructure are given by

$$\langle \boldsymbol{\varepsilon}^+ \rangle = \mathbf{S}^+ \langle \boldsymbol{\sigma}^+ \rangle, \quad \langle \boldsymbol{\varepsilon}^- \rangle = \mathbf{S}^- \langle \boldsymbol{\sigma}^- \rangle \tag{10}$$

where \mathbf{S} is the compliance tensor ($\mathbf{S} \equiv \mathbf{C}^{-1}$). With these relations, it is possible to define the stress concentration matrices [21]

$$\mathbf{B}^+ = \frac{(\mathbf{S}^+ - \mathbf{S}^-)^{-1}(\mathbf{S}^H - \mathbf{S}^-)}{\rho}, \quad \mathbf{B}^- = \frac{-(\mathbf{S}^+ - \mathbf{S}^-)^{-1}(\mathbf{S}^H - \mathbf{S}^+)}{1 - \rho} \tag{11}$$

Thus, the average stress in each phase inside the microstructure is evaluated as a function of the ‘homogenized stress’ $\langle \boldsymbol{\sigma} \rangle$ by

$$\langle \boldsymbol{\sigma}^+ \rangle = \mathbf{B}^+ \langle \boldsymbol{\sigma} \rangle, \quad \langle \boldsymbol{\sigma}^- \rangle = \mathbf{B}^- \langle \boldsymbol{\sigma} \rangle \tag{12}$$

In this work, the Von Mises failure function is adopted, and it is considered in each phase of the material inside the microstructure. Thus,

$$\langle \boldsymbol{\sigma}_{vm}^+ \rangle = \sqrt{\langle (\boldsymbol{\sigma})^T (\mathbf{B}^+)^T \mathbf{V} \mathbf{B}^+ \boldsymbol{\sigma} \rangle}, \quad \langle \boldsymbol{\sigma}_{vm}^- \rangle = \sqrt{\langle (\boldsymbol{\sigma})^T (\mathbf{B}^-)^T \mathbf{V} \mathbf{B}^- \boldsymbol{\sigma} \rangle} \tag{13}$$

where \mathbf{V} is given by

$$\mathbf{V} = \begin{bmatrix} 1 & -1/2 & -1/2 & 0 \\ -1/2 & 1 & -1/2 & 0 \\ -1/2 & -1/2 & 1 & 0 \\ 0 & 0 & 0 & 3 \end{bmatrix} \tag{14}$$

For simplicity, the square of Von Mises failure function is used as defined by

$$\langle \boldsymbol{\sigma}_{vm^2}^+ \rangle = \langle \boldsymbol{\sigma}_{vm}^+ \rangle^2 \quad \text{and} \quad \langle \boldsymbol{\sigma}_{vm^2}^- \rangle = \langle \boldsymbol{\sigma}_{vm}^- \rangle^2 \tag{15}$$

Thus, to be comparable, the admissible stress is also squared, i.e.

$$\langle \boldsymbol{\sigma}_{adm^2}^+ \rangle = \langle \boldsymbol{\sigma}_{adm}^+ \rangle^2 \quad \text{and} \quad \langle \boldsymbol{\sigma}_{adm^2}^- \rangle = \langle \boldsymbol{\sigma}_{adm}^- \rangle^2 \tag{16}$$

5. PROBLEM FORMULATION

A theoretical formulation for the topology optimization problem considering stress constraints was proposed by Duysinx and Bendsøe [9]. These authors pointed out two important facts about dealing with stress constraint in the layout optimization of continuum structures: (a) the need for taking into account the stress in the microstructure and (b) the *stress singularity phenomenon* (SSP). The stress in the microstructure was also treated by Lipton [29], who presented a formulation to design functionally graded reinforced shafts subjected to torsional loads, and by Allaire *et al.* [30], who applied topology optimization to minimize an integral of the stress over the domain.

The *stress singularity phenomenon* or SSP, pointed out by Sved and Ginos [10], occurs in layout optimization problems when the material volume fraction of a region in the structure tends

to vanish and the micro-stress in this region remains finite. Thus, if the micro-stress value is larger than the limiting stress value the optimization procedure will not be able remove material from this region and reach the lower volume fraction bound. This problem was treated, from the numerical point of view for the continuum problem, by Pereira *at al.* [11] where the concepts of ε -relaxation, proposed by Cheng and Guo [13] for truss problems, and by Duysinx and Bendsøe [9] for continuum problems.

Considering the optimization problem of minimizing the volume of phase + with stress constraint, we propose the first formulation considering two local constraints for stresses in each material phase, i.e.

$$\begin{aligned} & \min_{\rho} \int_{\Omega} \rho(x) \, d\Omega \\ & \text{such that } \frac{\langle \boldsymbol{\sigma}_{\text{vm}^2}^+ \rangle}{\langle \boldsymbol{\sigma}_{\text{adm}^2}^+ \rangle} \leq 1, \quad \frac{\langle \boldsymbol{\sigma}_{\text{vm}^2}^- \rangle}{\langle \boldsymbol{\sigma}_{\text{adm}^2}^- \rangle} \leq 1 \end{aligned} \quad (17)$$

where Ω represents the *extended design domain*. Even though this formulation is strictly to prevent failure of both material phases, it presents the undesirable *stress singularity phenomenon*—the stresses in the material phases, given by relations (12), tend to finite values when the volumetric density tends to either zero or one. It is important to note that, differently from the layout (0–1) problem, the material distribution problem can be defined to avoid the *stress singularity phenomenon* because the material does not vanish, and thus, every point of the *extended design domain* can have finite stress. This approach was adopted by Lipton [29].

Therefore, to avoid *stress singularity phenomenon*, a unique stress failure criterion is proposed based on the arithmetic mean of the Von Mises stress:

$$\langle \boldsymbol{\sigma}_{\text{vm}^2}^{\text{micro}} \rangle = \rho \langle \boldsymbol{\sigma}_{\text{vm}^2}^+ \rangle + (1 - \rho) \langle \boldsymbol{\sigma}_{\text{vm}^2}^- \rangle \quad (18)$$

This new Von Mises stress in the microstructure has the advantage that when one of the phases is vanishing, the stress tends to the Von Mises stress at the other phase. Thus, the SSP is avoided. Substituting Equations (13) in (18), it is possible to define the matrix \mathbf{B}_{vm} by

$$\mathbf{B}_{\text{vm}} = \rho (\mathbf{B}^+)^T \mathbf{V} \mathbf{B}^+ + (1 - \rho) (\mathbf{B}^-)^T \mathbf{V} \mathbf{B}^- \quad (19)$$

and thus,

$$\langle \boldsymbol{\sigma}_{\text{vm}^2}^{\text{micro}} \rangle = \langle \boldsymbol{\sigma} \rangle^T \mathbf{B}_{\text{vm}} \langle \boldsymbol{\sigma} \rangle \quad (20)$$

The advantage of considering the modified stress concentration factor \mathbf{B}_{vm} is that it tends to the matrix \mathbf{V} for ρ tending to 0 and 1. Thus, the following relations hold true (avoiding the SSP):

$$\lim_{\rho \rightarrow 1} \langle \boldsymbol{\sigma}_{\text{vm}^2}^{\text{micro}} \rangle = \langle \boldsymbol{\sigma}_{\text{vm}^2}^+ \rangle, \quad \lim_{\rho \rightarrow 0} \langle \boldsymbol{\sigma}_{\text{vm}^2}^{\text{micro}} \rangle = \langle \boldsymbol{\sigma}_{\text{vm}^2}^- \rangle \quad (21)$$

Furthermore, to consider a unique stress failure criterion it is necessary to propose a unified admissible stress. In this work, the model proposed by Swan and Kosaka [31, 32] is considered. This approach, which is based on the harmonic mean of the admissible stress in each phase, was adopted because it tends to produce conservative results. In this model, the admissible stress is close to the admissible stress of the weak phase for a large range of volumetric densities. Thus,

the unified admissible stress is given by

$$\langle \sigma_{adm^2}^{micro} \rangle \equiv \left[\frac{\rho}{\langle \sigma_{adm^2}^+ \rangle} + \frac{1-\rho}{\langle \sigma_{adm^2}^- \rangle} \right]^{-1} \tag{22}$$

Thus, the stress constraint in the original problem (17) is re-written in the form:

$$\frac{\langle \sigma_{vm^2}^{micro} \rangle}{\langle \sigma_{adm^2}^{micro} \rangle} - 1 < 0 \tag{23}$$

It is important make clear that, using an unified stress constraint, does not guarantee that the stress constraint in each phase, as defined in problem (17), will be satisfied.

From a numerical point of view, the above local constraint (23) is undesirable because of the high computational cost to evaluate the sensitivity for each constraint. To improve the computational efficiency, the first term of this constraint is substituted by a global equation:

$$\left[\frac{1}{\Omega} \int_{\Omega} \left(\frac{\langle \sigma_{vm^2}^{micro} \rangle}{\langle \sigma_{adm^2}^{micro} \rangle} \right)^p d\Omega \right]^{1/p} \tag{24}$$

where, in the limit when p tends to infinity, the local constraint is recovered.

Thus, considering changes of the optimization problem proposed to avoid the SSP and to improve computational efficiency, the following formulation is proposed:

$$\begin{aligned} & \min_{\rho, \beta} \int_{\Omega} \rho(x) d\Omega + \beta \\ & \text{such that} \quad \left[\frac{1}{\Omega} \int_{\Omega} \left(\frac{\langle \sigma_{vm^2}^{micro} \rangle}{\langle \sigma_{adm^2}^{micro} \rangle} \right)^p d\Omega \right]^{1/p} - \beta - 1 < 0 \end{aligned} \tag{25}$$

The parameter β is applied as relaxation of the constraint in the sense of mathematical programming. This formulation allows starting the problem from an unfeasible point of the design space, and it also allows a steep change of p -value during the optimization.

6. NUMERICAL IMPLEMENTATION

To solve the problem stated in (25) an axisymmetric finite element model is developed with a four-node bilinear element. Thus, the discretized formulation of the problem stated in (25) is given by

$$\begin{aligned} & \min_{\rho, \beta} \sum_{e=1}^M \int_{\Omega_e} \rho(x) d\Omega_e - \beta \\ & \text{such that} \\ & \left[\frac{1}{\Omega} \sum_{e=1}^M \Omega_e \left(\frac{\langle \sigma_{vm^2,e}^{micro} \rangle}{\langle \sigma_{adm^2,e}^{micro} \rangle} \right)^p \right]^{1/p} - \beta - 1 < 0 \end{aligned} \tag{26}$$

where Ω represents the volume of the *extended design domain* which is discretized by M finite elements, Ω_e represent the volume of element e , and the values of $\langle \sigma_{vm^2,e}^{\text{micro}} \rangle$ and $\langle \sigma_{adm^2,e}^{\text{micro}} \rangle$ are the stresses $\langle \sigma_{vm^2}^{\text{micro}} \rangle$ and $\langle \sigma_{adm^2}^{\text{micro}} \rangle$ evaluated at the center of the element e .

The continuum distribution of the volumetric density inside each element is given by the function

$$\rho(x) = \sum_{i=1}^4 \rho_i N_i \quad (27)$$

where ρ_i is the nodal volumetric density and N_i is the finite element shape function, chosen such that for $\rho_i > 0$ we also have $\rho(x) > 0$. The values of ρ_i must have a lower-bound greater than 0 and an upper-bound lower than 1 because of the fact that the functions (11), and consequently functions (19) and (20), are undefined for the values 1 and 0, respectively.

Because of the large number of design variables and the existence of constraint in the optimization problem, a mathematical programming method called sequential linear programming (SLP) is applied. The linearization of the optimization problem (Taylor Series) in each iteration requires the sensitivities of the objective function and constraint in relation to of each ρ_i of the mesh. The sensitivity analysis of the constraint is obtained by using the adjoint method. Because of the high non-linearity of the constraint, the change of the volumetric density must be bounded in each iteration. The moving limits, which define the upper and lower bounds of the design box constraint [33], are set from 0.01 to 5% of the design variable.

A continuation of the parameter p of Equation (24) is applied to avoid high non-linearities at the beginning of the optimization problem and to ensure the local stress representation of the global constraint at the end of the process. The continuation adopted for the p -value is defined on a case-by-case basis (for each example presented). The change of the p -value was controlled either by the maximum variation of volumetric nodal density ($\max\{\rho_i\} \leq 10^{-3}$) or the limit of n iterations, also defined for each example. To regularize the problem, a spatial filter, as proposed by Cardoso [34], was applied.

7. NUMERICAL EXAMPLES

This section presents two numerical examples to demonstrate the potential of the proposed method. The design of an FGM rotating disk, and the conceptual design of a turbine disk are discussed below. For the later example, both one- and two-dimensional material gradation variation are investigated.

7.1. Example 1—FG rotating disk

The example illustrated by Figure 3 introduces a distributed body force due to rotation of the disk. The example considers the *extended design domain* of Figure 4 (with corresponding boundary condition) as a quarter part of geometry of the entire disk represented in Figure 3. The axisymmetry and symmetry of the geometry are considered.

The disk is subjected only to the centrifugal forces due to a constant angular speed $\omega = 1$. The stiffest and the softest materials have the Young's modulus equal to 1 and 0.1, respectively. Both have the same Poisson's ratio, equal to 0.3, and the same density ($\rho^+ = \rho^- = 1$).

For this problem, the homogeneous disk presents a maximum Von Mises stress equal to 0.41 that is independent of the Young's modulus. In the first solution, the admissible Von Mises stress of

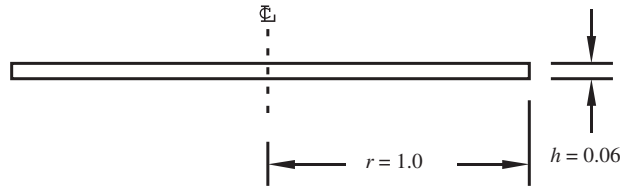


Figure 3. Geometry of the FG rotating disk problem.

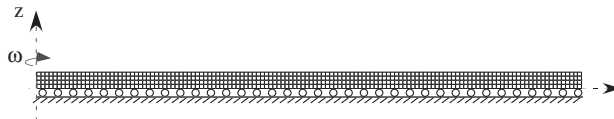


Figure 4. Mesh and boundary conditions for the axisymmetric problem.

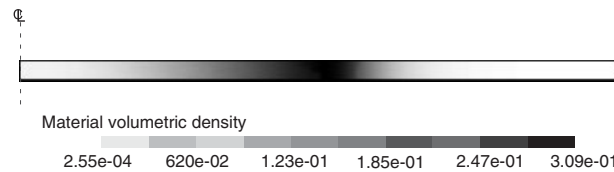


Figure 5. Solution of the material distribution problem.

both materials is set equal to 0.39 ($\langle \sigma_{adm}^- \rangle = \langle \sigma_{adm}^- \rangle = 0.39$). Note that the load applied to the disk, due to its rotation, remains unchanged because both materials have the same density. Applying the optimization procedure, and defining the variation of the p -value as $p_1 = 2$, $p_2 = 20$, $p_3 = 50$ and, $p_4 = 100$, we obtain the material distribution represented in Figure 5.

The material volumetric density ρ and the effective Young's modulus, given by the material model in terms of ρ , are plotted in Figure 6(a). In comparison with the homogeneous case, in the FGM case the soft material leads to a reduced stress in the inner part of the disk, which is due to the proper material distribution by the optimization algorithm. Figure 6(b) shows that the specific material distribution leads to maximum Von Mises stress distribution equal to 0.394, which violates the constraint in only 1%. This violation in the constraint is numerically admissible considering the global constraint adopted and the relaxation of the constraint by the parameter β . Thus, this method is able to provide an optimized material distribution for the functionally graded rotating disk that minimizes the amount of phase plus (+) and also satisfies the stress constraint within acceptable accuracy.

To better understand the behaviour of the stress constraint, given by Equation (23), the Von Mises stresses in each phase of the FGM are presented in Figure 7. In this graph, it shows that the Von Mises stress in phase 1 is above the admissible stress for radius smaller than approximately 0.65. However, the Von Mises stress in the micro-structure, given by Equation (20), follows the

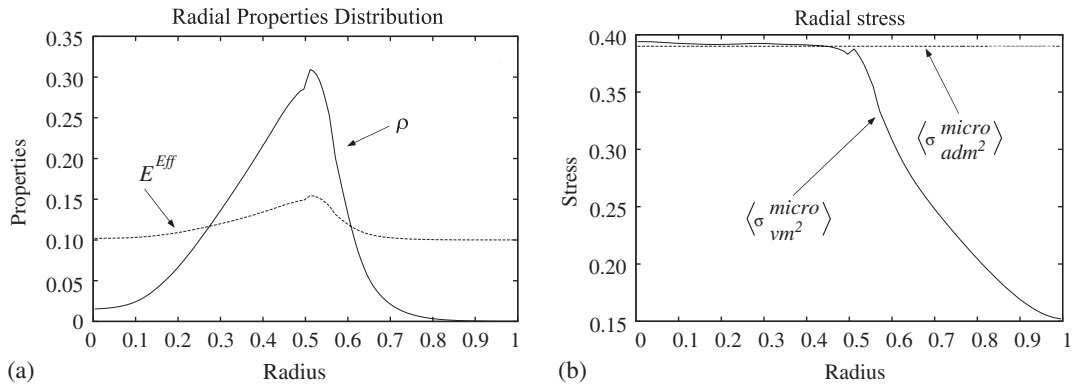


Figure 6. Material and Von Mises stress distribution along the radius of the FG rotating disk.

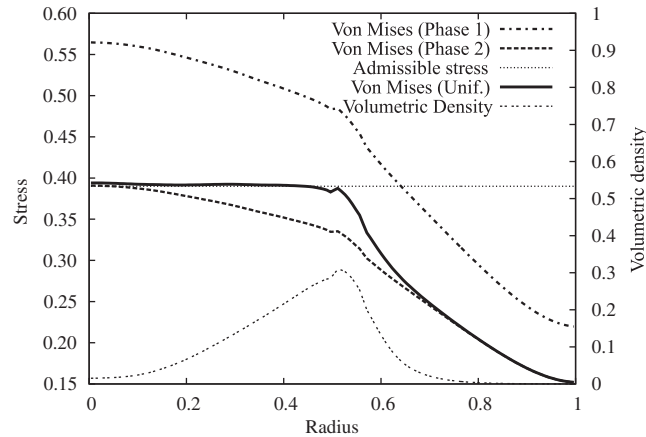


Figure 7. Von Mises stresses (phase 1, phase 2, and unified) and volumetric density along the radius of the FG rotating disk.

admissible stress from radius equal to zero to approximately 0.5, and then it starts to decrease until the rim of the disk. This behaviour is expected because we are using a unique stress criteria, given by Equation (23), and we do not expect that the Von Mises stress in each phase will be separately admissible.

Even though this unique stress criteria does not guarantee the admissible stress in each separate phase, it was proposed to avoid the SSP (see Figure 7). The Von Mises stress value on phase 1 for radius larger than 0.8 is around 0.25, however the volumetric density in this region is the lower bound 0.0002. The volumetric density of phase 1 in this region should be equal to zero and, as a consequence, the stress in this phase either would not be defined, or it should be equal to zero. However, when the volumetric density tends to zero, the stress tends to a finite value equal to 0.13. If this stress value is larger than the admissible stress value, the optimization method cannot

remove this material phase, characterizing the SSP. Indeed, by considering the Von Mises stress in the micro-structure as proposed in this work, we notice that when one of the phases tends to vanish, the stress tends to the Von Mises stress of the remaining phase, which is physically sound.

7.2. Example 2—FG turbine disk

The second example is the conceptual design of a functionally graded turbine disk. The geometry and boundary conditions of the turbine disk is based on Reference [35]. The disk geometry is represented in Figure 8. The axisymmetry and symmetry in relation to the plane (x, z) are both considered. Thus, only the section in the plane (x, y) is depicted.

The turbine disk is subjected to three loads. An inner pressure $fp = 40$ MPa resulting from the disk and shaft fit which acts radially, shown in Figure 8. On the outer side of the disk there is an uniform distributed load, $bp = 200$ MPa due to the blades, which acts radially outwards from the rotation axis. The disk is also subjected to rotation speed of $\omega = 2000$ rpm that generates a centrifugal load distributed in the disk body.

In this example, two fictitious material were chosen, one called ‘C’, that represents the ceramic material, and another, called ‘A’, representing engineering alloys (such as, Ni-alloy, Mo-alloys, among others). The mechanical properties of these basic materials are presented in Table I [36]. In order to compare the result of the turbine disk with the optimized functionally graded material distribution, the failure function given by Equation (23) for a homogeneous turbine disk with material ‘C’ and one with material ‘A’ were analysed. The disk made of material ‘C’ has the maximum Von Mises stress 23 times below the admissible stress of its material, and the disk with material

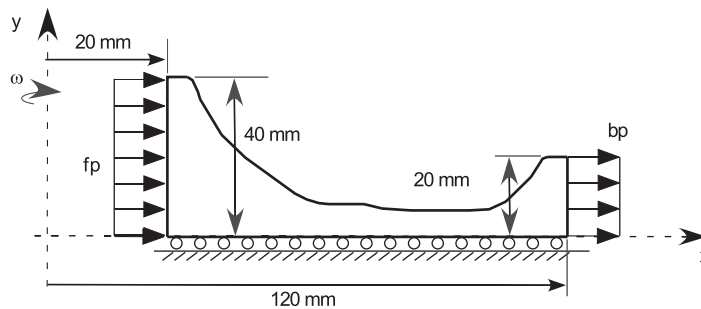


Figure 8. Schematic representation of the geometry and boundary conditions of the turbine disk.

Table I. Mechanical properties [36].

Properties	Material (+)	Material (–)
	‘C’	‘A’
Density (kg/m ³)	4000	9000
Young’s modulus (GPa)	350	110
Poisson’s ratio	0.25	0.3
Strength (MPa)	3500	300

'A' has the maximum Von Mises stress 8 times higher than the admissible stress of material 'A'. Thus, the task of the optimization procedure consists of finding a material distribution with the minimum amount of material 'C' that satisfies the admissible stress. Applying the optimization procedure defining the variation of the p -value as $p_1 = 15$, $p_2 = 30$, $p_3 = 60$, and $p_4 = 120$, and using a filter with radius equal to 1 mm, we obtain result presented in Plate 1. The failure function stress field is presented in Plate 2. Notice that the maximum Von Mises stress is only 5% above the admissible stress. As in the previous example, this constraint violation is numerically admissible as it is a global stress constraint.

Now, suppose that the manufacturing process is limited to produce only one-dimensional material gradation, e.g. along the horizontal axis. Thus, the turbine disk material distribution was optimized allowing only x -direction gradation. In this example, a continuation for the p -value was defined as $p_1 = 15$, $p_2 = 30$, $p_3 = 90$ and $p_4 = 150$. As before, a filter with radius equal to 1 mm is employed. The result obtained is presented in Plate 3.

The material distribution for the turbine disk with only x -direction gradation, produces a maximum failure function equal to 1.05, which represents a Von Mises stress value only 5% above the admissible stress. The failure function stress field is presented in Plate 4. As indicated before, such result is numerically admissible. This maximum stress value is equal to the example of two-dimensional gradation (Plate 1), however the volume of material 'C' necessary to achieve this stress level is larger. The x -direction gradation has a volume fraction of material 'C' equal to 77%, while the two-dimensional gradation has 61%. Computationally, such difference can be explained by considering that x -direction gradation is a constraint that limits the feasible space of the optimization problem.

8. CONCLUDING REMARKS

Topology optimization with stress constraints is a viable and powerful technique for preliminary design of functionally graded structures. To properly account for spatial tailoring of material properties, we employ the 'continuous approximation of material distribution' (CAMD) approach. The present formulation for stress concentration factor avoids the undesirable *stress singularity phenomenon* or SSP. The material model consists of a non-linear interpolation between the Hashin–Strikman upper and lower bounds. However, the formulation is general and it can be used with other material models. Finally, the numerical results demonstrate that the method generates smooth material distributions and is able to satisfy the stress constraint within acceptable degree of accuracy.

APPENDIX A: HASHIN–STRIKMAN (HS) BOUNDS

The upper and lower Hashin–Strikman (HS) bounds for the bulk modulus (K) are given by [8, 19]

$$K_{\text{upper}} = (1 - \rho)K^- + \rho K^+ - \frac{(1 - \rho)\rho(K^+ - K^-)^2}{(1 - \rho)K^+ + \rho K^- + G^+} \quad (\text{A1})$$

and

$$K_{\text{lower}} = (1 - \rho)K^- + \rho K^+ - \frac{(1 - \rho)\rho(K^+ - K^-)^2}{(1 - \rho)K^+ + \rho K^- + G^-} \quad (\text{A2})$$

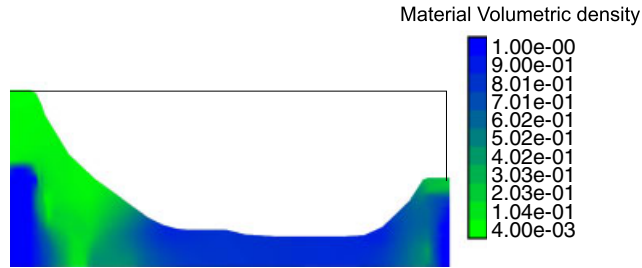


Plate 1. Material distribution for the FG turbine disk.

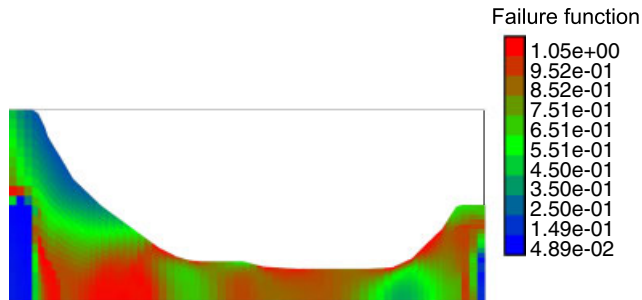


Plate 2. Failure function of the FG turbine disk—see Equation (23).

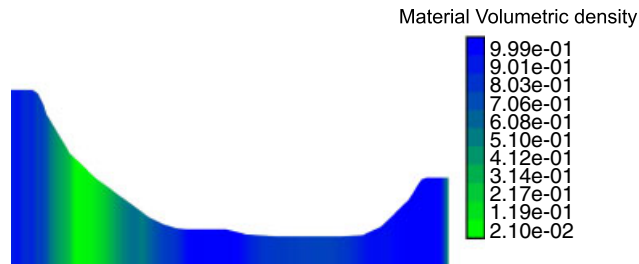


Plate 3. Material distribution considering x -direction gradation for the FG turbine disk.

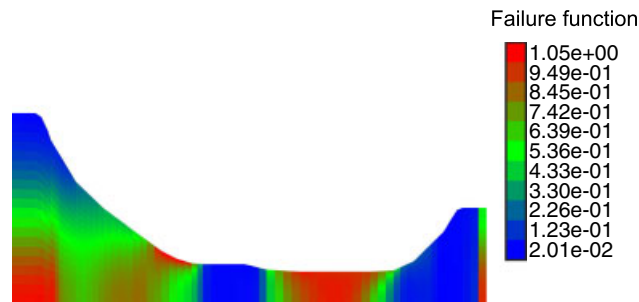


Plate 4. Failure function considering x -direction gradation for the FG turbine disk—see Equation (23).

and the bounds for the shear modulus (G) by

$$G_{\text{upper}} = (1 - \rho)G^- + \rho G^+ - \frac{(1 - \rho)\rho(G^+ - G^-)^2}{(1 - \rho)G^+ + \rho G^- + \frac{K^+ G^+}{K^+ + 2G^+}} \quad (\text{A3})$$

and

$$G_{\text{lower}} = (1 - \rho)G^- + \rho G^+ - \frac{(1 - \rho)\rho(G^+ - G^-)^2}{(1 - \rho)G^+ + \rho G^- + \frac{K^- G^-}{K^- + 2G^-}} \quad (\text{A4})$$

APPENDIX B: NOMENCLATURE

List of symbols

\mathbf{C}^{Eff}	stiffness tensor of the mixture
$\mathbf{C}^+, \mathbf{C}^-$	stiffness tensor of material + and -, respectively
ρ	volumetric density of material +
p	penalization parameter for the SIMP
$K_{\text{upper}}, K_{\text{lower}}$	Hashin–Strikman upper and lower bulk modulus, respectively
$G_{\text{upper}}, G_{\text{lower}}$	Hashin–Strikman upper and lower shear modulus, respectively
K^+, K^-	bulk modulus of material + and -, respectively
G^+, G^-	shear modulus of material + and -, respectively
$\varphi(\cdot)$	interpolation function of HS bounds
ρ^{Eff}	material density of the mixture
ρ^+, ρ^-	density of material + and -, respectively
$\boldsymbol{\sigma}$	stress tensor
V	volume of the RVE
\mathbf{y}	coordinate system of the RVE
$\boldsymbol{\varepsilon}$	strain tensor
$\langle \cdot \rangle$	mean of the corresponding quantity
$\mathbf{S}^+, \mathbf{S}^-$	compliance tensor of material + and -, respectively
$\mathbf{B}^+, \mathbf{B}^-$	stress concentration of phases + and -, respectively
$\langle \boldsymbol{\sigma}_{\text{vm}}^+ \rangle$	Von Mises stress on phase +
$\langle \boldsymbol{\sigma}_{\text{vm}}^- \rangle$	Von Mises stress on phase -
$\langle \boldsymbol{\sigma}_{\text{vm}^2}^+ \rangle$	square of the Von Mises stress on phase +
$\langle \boldsymbol{\sigma}_{\text{vm}^2}^- \rangle$	square of the Von Mises stress on phase -
$\langle \boldsymbol{\sigma}_{\text{adm}^2}^+ \rangle$	square of the admissible stress on phase +
$\langle \boldsymbol{\sigma}_{\text{adm}^2}^- \rangle$	square of the admissible stress on phase -
$\langle \boldsymbol{\sigma}_{\text{vm}^2}^{\text{micro}} \rangle$	square of the Von Mises stress on the microstructure
\mathbf{B}_{vm}	modified stress concentration matrices
$\langle \boldsymbol{\sigma}_{\text{adm}^2}^{\text{micro}} \rangle$	square of the admissible stress on the microstructure
β	variable for constraint relaxation
ρ_i	nodal volumetric density of material +
N_i	finite element shape function

ACKNOWLEDGEMENTS

The first author thanks CNPq (Conselho Nacional de Desenvolvimento Científico e Tecnológico), for the MS fellowship (no.131436/2004-0). We also acknowledge the grant from the University of São Paulo (USP), FAPESP (Fundação de Amparo à Pesquisa do Estado de São Paulo), CAPES (Coordenação de Aperfeiçoamento de Pessoal de Nível Superior), the USA NSF through the project CMS#0303492 (Inter-Americas Collaboration in Materials Research and Education, PI Prof. W. Soboyejo, Princeton University), and the Midwest Structural Science Center (MSSC) at the University of Illinois at Urbana-Champaign (UIUC) through the Air Force Research Laboratory (AFRL).

REFERENCES

1. Cho JR, Choi JH. A yield-criteria tailoring of the volume fraction in metal-ceramic functionally graded material. *European Journal of Mechanics – A/Solids* 2004; **23**(2):271–281.
2. Durodola JF, Attia O. Deformation and stresses in functionally graded rotating disks. *Composites Science and Technology* 2000; **60**(7):987–995.
3. Horgan CO, Chan AM. The stress response of functionally graded isotropic linearly elastic rotating disks. *Journal of Elasticity* 1999; **55**(3):219–230.
4. Turteltaub S. Functionally graded materials for prescribed field evolution. *Computer Methods in Applied Mechanics and Engineering* 2002; **191**(21–22):2283–2296.
5. Paulino GH, Silva ECN. Design of functionally graded structures using topology optimization. *Materials Science Forum* 2005; **492–493**:435–440.
6. Stump FV. Otimização topológica aplicada ao projeto de estruturas tradicionais e estruturas com gradação funcional sujeitas a restrição de tensão. *MS Thesis*, Universidade de São Paulo, Brazil, 2006.
7. Bendsoe MP, Kikuchi N. Generating optimal topologies in structural design using a homogenization method. *Computer Methods in Applied Mechanics and Engineering* 1988; **71**(2):197–224.
8. Bendsoe MP, Sigmund O. *Topology Optimization: Theory Methods and Applications*. Springer: Berlin, 2003.
9. Duysinx P, Bendsoe MP. Topology optimization of continuum structures with local stress constraints. *International Journal for Numerical Methods in Engineering* 1998; **43**(8):1453–1478.
10. Sved G, Ginos Z. Structural optimization under multiple loading. *International Journal of Mechanical Sciences* 1968; **10**(10):803–805.
11. Pereira JT, Fancello EA, Barcellos CS. Topology optimization of continuum structures with material failure constraints. *Structural and Multidisciplinary Optimization* 2004; **26**(1–2):50–66.
12. Yang RJ, Chen CJ. Stress-based topology optimization. *Structural Optimization* 1996; **12**(2–3):98–105.
13. Cheng GD, Guo X. ϵ -Relaxed approach in structural topology optimization. *Structural Optimization* 1997; **13**(4):258–266.
14. Allaire G. *Shape Optimization by the Homogenization Method*. Series: Applied Mathematical Sciences, vol. 146. Springer: New York, 2002.
15. Torquato S. *Random Heterogeneous Materials: Microstructure and Macroscopic Properties*. Series: Interdisciplinary Applied Mathematics, vol. 16. Springer: New York, 2002.
16. Matsui K, Terada K. Continuous approximation of material distribution for topology optimization. *International Journal for Numerical Methods in Engineering* 2004; **59**(14):1925–1944.
17. Rahmatalla S, Swan CC. Form finding of sparse structures with continuum topology optimization. *Journal of Structural Engineering (ASCE)* 2003; **129**(12):1707–1716.
18. Kim JH, Paulino GH. Isoparametric graded finite elements for nonhomogeneous isotropic and orthotropic materials. *Journal of Applied Mechanics—Transactions of the ASME* 2002; **69**(4):502–514.
19. Hashin Z, Shtrikman S. A variational approach to the theory of the elastic behaviour of multiphase materials. *Journal of the Mechanics and Physics of Solids* 1963; **11**:127–140.
20. Zuiker J, Dvorak G. The effective properties of functionally graded composites. I. Extension of the Mori–Tanaka method to linearly varying fields. *Composites Engineering* 1994; **4**:19–35.
21. Reiter T, Dvorak GJ, Tvergaard V. Micromechanical models for graded composite materials. *Journal of the Mechanics and Physics of Solids* 1997; **45**:1281–1302.
22. Reiter T, Dvorak GJ. Micromechanical models for graded composite materials: II. Thermomechanical loading. *Journal of the Mechanics and Physics of Solids* 1998; **46**(9):1655–1673.

23. Tanaka K, Watanabe H, Sugano Y, Poterasu V. A multicriterial material tailoring of a hollow cylinder in functionally graded materials: scheme to global reduction of thermoelastic stresses. *Computer Methods in Applied Mechanics and Engineering* 1996; **135**(3–4):369–380.
24. Kim JH, Paulino GH. An accurate scheme for mixed-mode fracture analysis of functionally graded materials using the interaction integral and micromechanics models. *International Journal for Numerical Methods in Engineering* 2003; **58**(10):1457–1497.
25. Zuiker JR. Functionally graded materials: choice of micromechanics model and limitations in property variation. *Composites Engineering* 1995; **5**:807–819.
26. Aboudi J, Pindera MJ, Arnold SM. Higher-order theory for functionally graded materials. *Composites Part B—Engineering* 1999; **30**(8):777–832.
27. Yin HM, Sun LZ, Paulino GH. Micromechanics-based elastic model for functionally graded materials with particle interactions. *Acta Materialia* 2004; **52**(12):3535–3543.
28. Benveniste Y. A new approach to the application of Mori–Tanaka’s theory in composite materials. *Mechanics of Materials* 1987; **6**:147–157.
29. Lipton R. Design of functionally graded composite structures in the presence of stress constraints. *International Journal of Solids and Structures* 2002; **39**(9):2575–2586.
30. Allaire G, Jouve F, Maillot H. Topology optimization for minimum stress design with the homogenization method. *Structural and Multidisciplinary Optimization* 2004; **28**(2–3):87–98.
31. Swan CC, Kosaka I. Voigt-Reuss topology optimization for structures with linear elastic material behaviours. *International Journal for Numerical Methods in Engineering* 1997; **40**(16):3033–3057.
32. Swan CC, Kosaka I. Voigt-Reuss topology optimization for structures with nonlinear material behaviours. *International Journal for Numerical Methods in Engineering* 1997; **40**(20):3785–3814.
33. Vanderplaats GN. *Numerical Optimization Techniques for Engineering Design*. McGraw-Hill: New York, 2002.
34. Cardoso EL. Controle de complexidade na otimização topológica de estruturas contínuas. *MS Thesis*, Universidade Federal do Rio Grande do Sul, Brazil, 2000.
35. Liu JS, Parks GT, Clarkson PJ. Optimization of turbine disk profiles by metamorphic development. *Journal of Mechanical Design* 2002; **124**(2):192–200.
36. Ashby MF. *Materials Selection in Mechanical Design*. Butterworth-Heinemann: Stoneham, MA, 1999.